electronic reprint

Acta Crystallographica Section B
Structural Science
ISSN 0108-7681

Modulated structure of $La_2Co_{1.7}$ from neutron and X-ray diffraction data

Michal Dusek, Gervais Chapuis, Penelope Schobinger-Papamantellos, Clive Wilkinson, Vaclav Petricek, L. D. Tung and Karl Heinz Juergen Buschow

Acta Crystallographica Section B
Structural Science
ISSN 0108-7681

Modulated structure of $La_2Co_{1.7}$ from neutron and X-ray diffraction data

Michal Dusek,[a,b]* Gervais Chapuis,[a] Penelope Schobinger-Papamantellos,[c] Clive Wilkinson,[d,e] Vaclav Petricek,[b] L. D. Tung[f,g] and Karl Heinz Juergen Buschow[g]

[a]Université de Lausanne, Institut de Cristallographie, BSP Dorigny, CH-1015 Lausanne, Switzerland, [b]Institute of Physics, Academy of Sciences of the Czech Republic, Na Slovance 2, 182 21 Praha 8, Czech Republic, [c]Laboratorium für Kristallographie, ETHZ CH-8092 Zürich, Switzerland, [d]Department of Physics, King's College London, Strand, London WC2R 2LS, England, [e]Institute Laue Langevin (ILL), Avenue des Martyrs, BP156, 38042 Grenoble CEDEX 9, France, [f]International Training Institute for Materials Science-ITIMS, 1 Dai Co Viet Str., Hanoi, Vietnam, and [g]Van der Waals-Zeeman Institute, University of Amsterdam, Valckenierstrasse, 651018 XE Amsterdam, The Netherlands

Correspondence e-mail: dusek@fzu.cz

Received 17 April 2000
Accepted 14 August 2000

An $La_2Co_{1.7}$ crystal was investigated by single-crystal neutron and X-ray diffraction. The neutron measurement was performed with a Laue white-beam technique at 15 K and room temperature, using a large position-sensitive detector. The X-ray measurements were obtained at room temperature from a CCD detector. The average structure of $La_2Co_{1.7}$ is hexagonal with cell parameters a = 4.885 (1), c = 4.273 (2) Å and space group $P6_3/mmc$. The satellites are located at the vertices of small hexagons perpendicular to the c axis. The modulated crystal was indexed assuming a sixfold twinned 3 + 1 dimensional structure with $q = (\alpha, 0, \gamma)$. The structure was solved in the pseudoorthorhombic cell, with a = 8.461 (1), b = 4.885 (1), c = 4.273 (2) Å, in the superspace group $C2/m(\alpha, 0, \gamma)$. Owing to space requirements, the Co atoms cannot fit precisely into the octahedral sites of the La h.c.p. (hexagonal close packing). Instead, the Co atoms adopt a different periodicity, which is not commensurate with the periodicity of the La atoms. Two structure models have been refined in order to describe this behaviour, one using the sawtooth function for the positional modulation of cobalt and the other describing the structure as a composite system. The chemical composition calculated from the composite model is $La_2Co_{1.8\ (1)}$ with the estimated standard deviation arising from the variation of **q** for different samples. In both models lanthanum is incommensurately modulated, while the position of cobalt seems not to be affected by any relative periodic displacement.

1. Introduction

The first compounds of the type $R_2Co_{1.7}$, where R is a light rare-earth element, were prepared by Schweizer *et al.* (1971). They reported $Pr_2Co_{1.7}$ and $Nd_2Co_{1.7}$ synthesized by arc melting of the component metals and by annealing in vacuum at 773 K. They studied the crystals by X-ray powder diffraction techniques and found a hexagonal cell with R atoms at $(\frac{2}{3}, \frac{1}{3}, \frac{1}{4})$ and $(\frac{1}{3}, \frac{2}{3}, \frac{3}{4})$, and with cobalt forming columns along the c axis. The problem of the structure was that two Co atoms could not coexist at (0,0,0) and $(0,0,\frac{1}{2})$, as expected in the hexagonal close packing $ABAB$ of the rare-earth element, because the c period was too short (4.07 Å). This observation together with the presence of equidistant weak diffuse layers perpendicular to $\mathbf{c}^*$, led to the hypothesis that cobalt had its own periodicity along the c axis, which is incommensurate with the periodicity of the rare-earth element.

Very soon the third compound of the family, $La_2Co_{1.7}$, was synthesized. Ballou *et al.* (1986*a*,*b*) studied the magnetic properties of $R_2Co_{1.7}$ crystals and found that $La_2Co_{1.7}$ was antiferromagnetic, despite the fact that lanthanum does not

Table 1
Experimental details.

	Neutron LT data	Neutron RT data	X-ray RT data
Crystal data			
Chemical formula	$La_2Co_{1.8}$	$La_2Co_{1.8}$	$La_2Co_{1.8}$
Chemical formula weight	378	378	378
Temperature (K)	15	298/150	298
Cell setting	Monoclinic	Monoclinic	Monoclinic
Superspace group	$C2/m(\alpha 0\gamma)$	$C2/m(\alpha 0\gamma)$	$C2/m(\alpha 0\gamma)$
a (Å) hexagonal	4.8807 (1)	4.8857 (3)	4.895 (1)
c (Å) hexagonal	4.2723 (2)	4.2731 (3)	4.335 (1)
a (Å) monoclinic	8.45361 (1)	8.4622 (1)	8.478 (2)
b (Å) monoclinic	4.8807 (1)	4.8857 (3)	4.895 (1)
c (Å) monoclinic	4.2723 (2)	4.2731 (3)	4.335 (1)
β (°) monoclinic	90	90	90.00 (2)
a (Å) of Co composite subsystem	8.4707	8.4792	8.486
b (Å) of Co composite subsystem	4.8807	4.8857	4.895
c (Å) of Co composite subsystem	2.3775	2.3779	2.362
β (°) of Co composite subsystem	86.36	86.37	87.45
Modulation wavevector (hexagonal axis)	[0.113 (1),0,0.203 (2)]	[0.113 (1),0,0.203 (2)]	[0.080 (1),0,0.165 (1)]
Modulation wavevector (monoclinic axis)	[0.226 (1),0,0.203 (2)]	[0.226 (1),0,0.203 (2)]	[0.160 (1),0,0.165 (1)]
Modulation wavevector (Co subsystem)	(0.126,0,−0.444)	(0.126,0,−0.444)	(0.087,0,−0.455)
Z (hexagonal axis)	1	1	1
Z (monoclinic axis)	2	2	2
D_x (Mg m^{-3})	7.106	7.106	6.975
Crystal form	Cube	Cube	Bar
Crystal size (mm)	3 × 3 × 3	3 × 3 × 3	0.08 × 0.08 × 0.2
Crystal colour	Black	Black	Black
Data collection			
Diffractometer	LADI	LADI	KUMA
Detector	Imaging plate	Imaging plate	KUMA CCD camera
Data collection method	White-beam Laue technique	White-beam Laue technique	CCD monochromatic experiment
Radiation type	Neutron	Neutron	X-ray Mo K-$L_{2,3}$
Wavelength (Å)	0.8–4.5	0.8–4.5	0.71073
μ (mm^{-1})	–	–	30.701
Absorption correction	None	None	Analytical
T_{min}, T_{max}	–	–	0.0180, 0.1830
No. of measured reflections	4581	3847	32260
Range of h,k,l,m (monoclinic axis)	$-14 \rightarrow h \rightarrow 14$ $-6 \rightarrow k \rightarrow 6$ $-5 \rightarrow l \rightarrow 8$ $-1 \rightarrow m \rightarrow 1$	$-14 \rightarrow h \rightarrow 14$ $-6 \rightarrow k \rightarrow 6$ $-5 \rightarrow l \rightarrow 8$ $-1 \rightarrow m \rightarrow 1$	$-12 \rightarrow h \rightarrow 12$ $-5 \rightarrow k \rightarrow 6$ $-6 \rightarrow l \rightarrow 6$ $-2 \rightarrow m \rightarrow 2$
No. of observed reflections	2759	2033	7743
No. of independent reflections	2499	2226	9048
No. of independent main reflections	273	263	352
Criterion for observed reflections	$I > 3\sigma(I)$	$I > 3\sigma(I)$	$I > 3\sigma(I)$
R_{int}	0.1063	0.0941	0.1034
θ_{max} (°)	–	–	35.40
Refinement			
No. of reflections used in the refinement	2499	2226	4691
Refinement on	F	F	F
R, wR (all reflections)	0.1040, 0.1406	0.1198, 0.1695	0.2150, 0.2261
R, wR (main reflections)	0.0667, 0.0891	0.0603, 0.0766	0.0711, 0.1010
R, wR (satellites)	0.1475, 0.1780	0.2094, 0.2407	0.3545, 0.3028
S	3.45	4.18	16.83
No. of parameters	24	24	24
Weighting scheme	$[\sigma^2(F) + (0.02F)^2]^{-1}$	$[\sigma^2(F) + (0.02F)^2]^{-1}$	$[\sigma^2(F) + (0.005F)^2]^{-1}$
$(\Delta/\text{s.u.})_{max}$	0.0032	0.0005	0.0005
$\Delta\rho_{max}$ (e Å^{-3})	2.62	1.69	9.84
$\Delta\rho_{min}$ (e Å^{-3})	−3.12	−2.13	−9.26
Extinction correction	None	None	None
Source of atomic scattering factors	*International Tables for Crystallography* (1992, Vol. C)	*International Tables for Crystallography* (1992, Vol. C)	*International Tables for Crystallography* (1992, Vol. C)

carry a magnetic moment. The unique magnetic properties of $La_2Co_{1.7}$ were widely investigated (Ballou *et al.*, 1987; Nam *et al.*, 1998*a*,*b*), but the nuclear structure was always taken from Schweizer *et al.* (1971).

In a previous investigation, Wilkinson *et al.* (2000) confirmed the paramagnetic to antiferromagnetic transition near 146 K reported by Ballou *et al.* (1986*a*,*b*, 1987), Nam *et al.* (1998*a*,*b*) and Schweizer *et al.* (1971) from neutron diffraction results (T_N = 148 K) and magnetic measurements (T_N = 144 K). Our interest in this compound partly originated from its unique crystal structure consisting of rows of very closely spaced Co atoms along the *c* direction, while the Co—Co distances perpendicular to this direction are much larger. This could have opened the possibility that magnetic ordering does not disappear completely above T_N, but remains restricted to some ordering within the mentioned Co rows, with no magnetic coupling between the rows. Previous neutron data have refuted this possibility, however, showing that the Co moments completely disappear above T_N. Another interesting feature emerged from magnetic measurements. At temperatures well below T_N, there is a crossing of the two susceptibility curves measured in directions parallel and perpendicular to the *c* direction. This could be taken as an indication of a further magnetic phase transition below T_N.

The information given on the nuclear structure presented earlier by Schweizer *et al.* (1971) is in principle correct, but nowadays, following the development of the superspace formalism, a more detailed structure model can be proposed.

In the present study we report on the modulated atomic structure of $La_2Co_{1.7}$ solved from neutron and X-ray data at 15 K and room temperature. The neutron data were collected with the Laue white-beam technique (Wilkinson *et al.*, 2000), which is new for fast neutron data collection. This is the first attempt to solve an incommensurate structure from this type of measurement.

2. Experimental

2.1. Neutron data collection

The $La_2Co_{1.7}$ crystal (3 × 3 × 3 mm), cut from a single crystalline rod grown by means of a Travelling Solvent Floating Zone (TSFZ) technique, was measured with the Laue white-beam technique on the LADI neutron imaging plate diffractometer (Cipriani *et al.*, 1996). The data were collected at 15 K (later referenced as LT data in this article) and 295 K (RT data) with 30 min exposure time per frame with wavelengths between ~0.8 and 4.5 Å. The details of the neutron experiments are discussed in Wilkinson *et al.* (2000). The experimental details are given in Table 1.

Table 2
Comparison of internal *R* factors (%) for neutron and X-ray measurements.

The data are given in the form $(R_{int,obs})/(R_{int,all})$; $(N_{1,obs}/N_{1,all}) \rightarrow (N_{2,obs}/N_{2,all})$, where 'obs' means observed reflections, 'all' means all reflections, N_1 is the number of reflections before averaging, N_2 is the number of reflections after averaging.

	Neutron data, 15 K	Neutron data, 295 K	X-ray data, 295 K
All	0.106/0.106	0.093/0.094	0.095/0.103
	2760/4581 → 1643/2499	2032/3847 → 1280/2226	7743/32260 → 2451/9048
Main	0.088/0.088	0.081/0.081	0.071/0.071
	409/443 → 251/273	415/436 → 246/263	1088/1235 → 309/352
Satellites	0.188/0.188	0.199/0.200	0.210/0.247
	2351/4138 → 1392/2262	1617/3411 → 1034/1963	6655/31025 → 2144/8696

2.2. X-ray data collection

For the X-ray data collection we used the Kuma CCD four-circle diffractometer with the *KM4CCD* software package (Kuma Diffraction, 1999). The quality of the crystals was checked by simulating rotation photographs. More than 80 crystals were tested and most of them exhibited powder diffraction features. The best sample was selected on the basis of its size and the sharpness of the diffraction spots. The sample was measured with the highest possible detector distance of 125 mm in order to minimize the overlap of satellites. The exposure time per frame was 60–80 s, and the data were collected up to $\sin\theta/\lambda \simeq 0.8$.

2.3. Data processing and data quality

Table 2[1] shows the values of the internal *R* factors for the symmetry $P\bar{1}$. The value of R_{int} (calculated independently for each twin domain – see §2.4) indicates the poor quality of the internal agreement of satellite intensities for both neutron and X-ray data. For neutron data, the satellites were sharp and well separated (Fig. 1*a*), but their intensities were weak. The average of $I/\sigma(I)$, with $I/\sigma(I) > 3$, was 6.9 and 5.9 for the low- and room-temperature data sets, respectively. For the X-ray data, the satellite intensities were larger [the average of $I/\sigma(I)$, with $I/\sigma(I) > 3$, was 12.6] owing to the higher ratio between the scattering power of cobalt and lanthanum, but the diffraction spots were very broad and the first-order satellites were partially overlapping (see Fig. 1*b*). Moreover, the intensities were strongly affected by absorption. The crystal shape was measured with the *KM4CCD* software (Kuma Diffraction, 1999) and optimized by the *X-Shape* program (Stoe & Cie, 1996). The absorption correction, refinement and Fourier synthesis was carried out with *JANA*98 (Petricek & Dusek, 1998).

2.4. Diffraction pattern

The typical feature of the diffraction pattern of $La_2Co_{1.7}$ is the presence of hexagons formed by the first-order satellites around the main reflections with the sixfold axis parallel to the **c** axis. The hexagons are directly observed close to the main

[1] Supplementary data for this paper are available from the IUCr electronic archives (Reference: SN0005). Services for accessing these data are described at the back of the journal.

reflections in the neutron Laue diffractograms (Fig. 1*a*). Note the different intensities of the positive and negative satellites. In the X-ray measurement, the hexagons can be recognized in the reconstructed CCD images (Fig. 1*b*). The observed second-order satellites were too weak and therefore not included in the refinements.

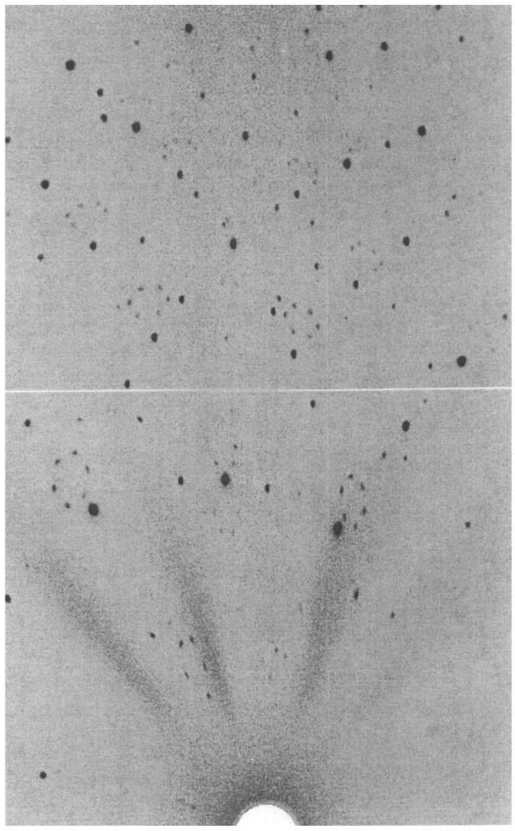

(*a*)

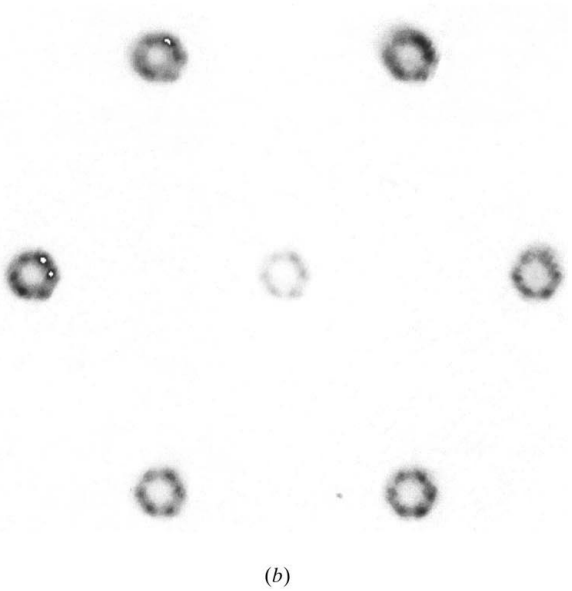

(*b*)

Figure 1
(*a*) Characteristic hexagons of satellites observed in the neutron diffraction experiment. (*b*) The plane (*h*,*k*,1.835) reconstructed from the CCD images with the *KM4CCD* software (Kuma Diffraction, 1999) shows the strongest first-order satellites.

The idealized hexagon of satellites is shown in Fig. 2. The six **q** vectors $(\alpha, 0, \gamma)$, $(0, \alpha, \gamma)$, $(-\alpha, \alpha, \gamma)$, $(-\alpha, 0, \gamma)$, $(0, -\alpha, \gamma)$ and $(\alpha, -\alpha, \gamma)$ can be described as a single **q** vector transformed by six twinning matrices. The necessary condition for this description – that the second-order satellites exist only in the direction of the first-order satellites – is fulfilled.

The refined **q** components were $q_x = 0.113$ (1), $q_y = 0$, $q_z = 0.203$ (2) and $q_x = 0.08$ (1), $q_y = 0$, $q_z = 0.165$ (1) for neutron and X-ray data, respectively. In the neutron measurement, no difference between **q** refined for low- and room-temperature data sets could be detected. Owing to the significant discrepancy between **q** refined for neutron and X-ray measurements, X-ray data were collected for another sample. The following values were obtained: $q_x = 0.06$ (1), $q_y = 0$, $q_z = 0.134$ (2). The length of the **q** vector most likely depends on the place in the crystalline rod from where the sample was extracted. Nevertheless, the common feature of all the samples tested is the presence of hexagons of satellites perpendicular to the *c* axis. The size of the satellite hexagon is defined by the length of the q_x component. This means that for very small q_x the satellites may overlap.

2.5. Symmetry

With a modulated vector **q** of the type $(\alpha, 0, \gamma)$, a monoclinic superspace group can be adopted. The space group of the average structure should therefore have a monoclinic subgroup, which preserves the cell content of the average structure and enables the same twinning operations (see Fig. 2). This is fulfilled for the space group $P6_3/mmc$ of the average structure and its subgroup $C2/m$. This subgroup will be used as the basic space group for the description of the modulated structure. The change of the symmetry from $P6_3/mmc$ to $C2/m$

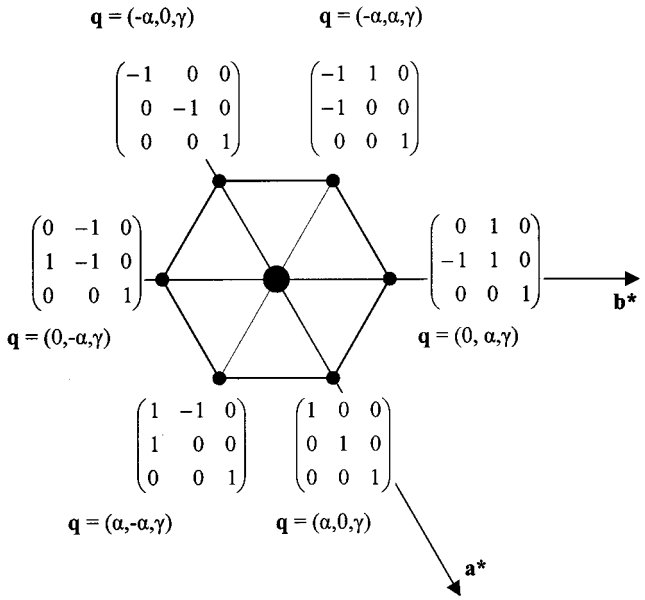

Figure 2
Idealized hexagon of satellites observed above and below the main reflections along with the twinning matrices used for the description of the one-dimensionally modulated structure with $q = (\alpha,0,\gamma)$.

Table 3
The non-weighted R factors, fractional atomic coordinates, equivalent isotropic displacement parameter (Å^2), the U^{33} component of anisotropic displacement parameters (Å^2) and the site occupation (O) for the average structure of La_2Co_{18}.

The symbols LT, RT and X represent neutron low-temperature, neutron room-temperature and X-ray room-temperature data.

Model	R	Atom	x	y	z	B_{eq}	U^{33}	O
LT	0.058	Co1				0.3 (1)	1.0 (4)	0.75 (6)
		Co2			0.5	0.3 (1)	1.0 (4)	0.75 (6)
		La	0.1649 (2)	0.5	0.2540 (4)	0.0065 (5)	0.0110 (3)	1
RT	0.049	Co1				0.25 (5)	0.7 (2)	0.74 (5)
		Co2			0.5	0.25 (5)	0.7 (2)	0.74 (5)
		La	0.1645 (2)	0.5	0.2520 (7)	0.0176 (5)	0.0246 (4)	1
X	0.058	Co1				0.282 (8)	0.78 (2)	0.941 (5)
		Co2			0.5	0.282 (8)	0.78 (2)	0.941 (5)
		La	0.1665 (1)	0.5	0.2431 (2)	0.0303 (5)	0.0392 (2)	1

is only possible after the transformation of the hexagonal cell to the pseudo-orthorhombic cell, using the relations $\mathbf{a}_{ort} = 2\mathbf{a}_{hex} + \mathbf{b}_{hex}$; $\mathbf{b}_{ort} = \mathbf{b}_{hex}$ and $\mathbf{c}_{ort} = \mathbf{c}_{hex}$.

3. Average and modulated structure

3.1. Refinement of the average structure

Lanthanum at (1/3, 2/3, 1/4) and cobalt at (0, 0, 0) form the average structure with the hexagonal space group $P6_3/mmc$. Both positions have multiplicity 2 and are completely fixed by symmetry. In the pseudo-orthorhombic cell with space group $C2/m$, lanthanum occupies the position (1/6, 1/2, 1/4) with multiplicity 4 and cobalt the positions (0, 0, 0) and (0, 0, 1/2), both with multiplicity 2. The average structure is shown in Fig. 3.

The average structure was refined in the monoclinic space group $C2/m$ in order to obtain the actual starting parameters for the refinement of the modulated structure. Although the x and z coordinates of lanthanum were free in this space group, the refined values were close to the positions in the hexagonal cell (see Table 3). A common feature observed for all data sets was the very large component U^{33} of the anisotropic displacement parameter of cobalt. The value close to 1 indicated that the electron/nuclear density is smeared along the c axis.

The two independent positions of cobalt at (0,0,0) and (0,0,$\frac{1}{2}$) are not the only possible ones in the average structure. The refinement with cobalt at (0,0,1/4), converged with a similar R value. Indeed the position of cobalt along the c axis is free, as indicated by the large displacement parameter U^{33}.

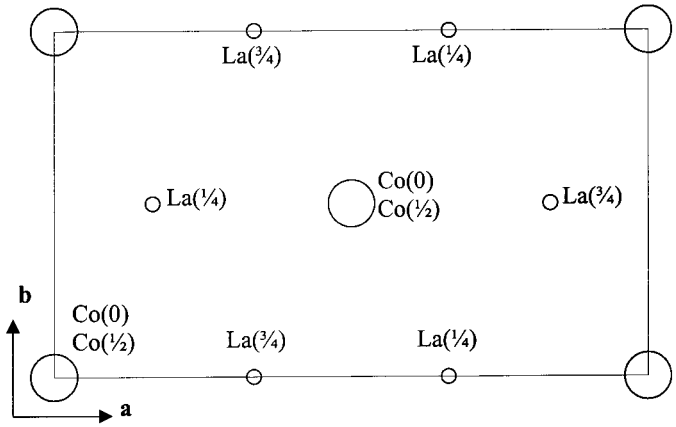

Figure 3
The average structure in the pseudo-orthorhombic cell with the fractional coordinates z given in parentheses.

Various refinements of the site occupancy of cobalt led to different compositions: $La_2Co_{1.50\,(6)}$, $La_2Co_{1.48\,(5)}$ and $La_2Co_{1.882\,(5)}$ for neutron low-temperature, neutron room-temperature and X-ray data, respectively. It should be noted, however, that these numbers are not necessarily meaningful, as the intensities of the satellite reflections have not been included. For an incommensurately modulated structure, the usual crystallographic fitting methods cannot provide the actual basic structural parameters with the main reflections only. In addition, for the neutron Laue data, the refinement of the occupancy of the Co sites is based on very few reflections. This arises from a combination of two effects. The first is that the large value of U^{33} for Co atoms indicates that the hkl reflections with non-zero l (the great majority) have virtually no Co contribution; their intensities arise almost entirely from La atoms (this is the model of Schweizer *et al.*, 1971). The estimate for the composition in the refinements of the average structure is therefore only based on a few $hk0$ reflections. The second effect is a low-order 'hole' in the Laue data (see Fig. 5) collected from a small unit cell using a wide wavelength band, since most low index reflections are superimposed in the Laue diagrams (Weisgerber & Helliwell, 1993). These effects are illustrated in Figs. 4(a) and (b) for the neutron diffraction case. A Fourier map (Fig. 4a) generated from the F_{obs} (or corresponding F_{calc}) coefficients shows almost no trace of the Co nuclei. In Fig. 4(b), a map generated from a complete set of F_{calc} coefficients, calculated from the refined basic structure up to $\sin\theta/\lambda = 0.9$, shows very clearly that the nuclear density of cobalt is smeared along the c axis. In the X-ray refinement, the column of electron density was visible in the Fourier maps generated both from F_{obs} and F_{calc} coefficients. For this reason, the X-ray data were used for the basic solution of the modulated structure (see §3.2.1), despite the fact that the precision of the satellite intensities was not optimal.

3.2. Composite and sawtooth model of modulated structure

The space requirements of the Co atom, the diffraction pattern (Fig. 11) and Fourier map calculated for the average structure (Fig. 4) strongly indicate that cobalt has a different

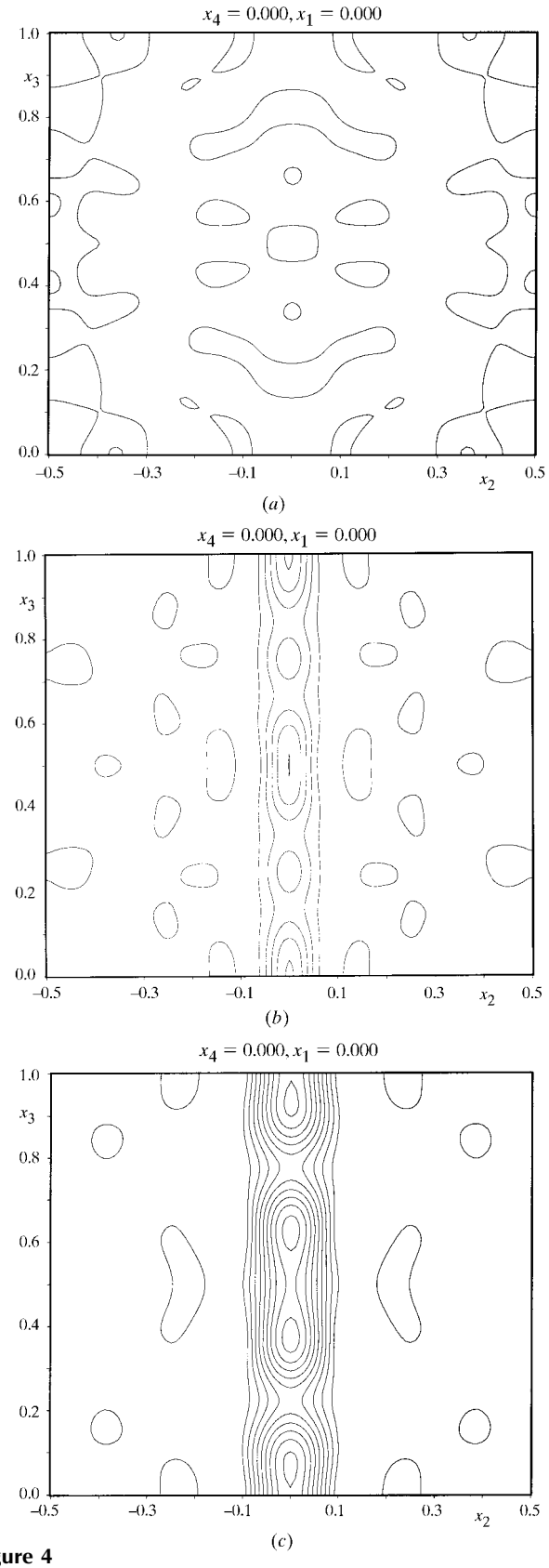

Figure 4
Sections of the three-dimensional Fourier map close to (0, 0, z). The contour step is 3 e Å^{-3}. (*a*) Fourier map with coefficients F_{obs} from the neutron low-temperature data; (*b*) neutron low-temperature data, Fourier map with coefficients F_{calc} generated up to $\sin\theta/\lambda = 0.9$; (*c*) X-ray data, Fourier map with coefficients F_{obs}.

periodicity than lanthanum along **c**. Two possible approaches are available in order to describe this type of structure.

3.2.1. Composite description. The most straightforward approach is the composite description where two subsystems with different cell parameters can be defined. The relationship of the subsystems is given by

$$\mathbf{H}^1 = \mathbf{H}^2\mathbf{W}, \tag{1}$$

where $\mathbf{H}^1$ and $\mathbf{H}^2$ are indices of the first and the second subsystem, respectively, $\mathbf{W}$ is a 4×4 transformation matrix. In the composite description, lanthanum is in the first subsystem, which is identical with the elementary cell of the average structure. In the second subsystem, cobalt can be placed in a smaller cell with a **c** parameter corresponding to the expected periodicity. The second subsystem must be recognizable in reciprocal space.

3.2.2. Sawtooth description. Another approach for cobalt to achieve a proper Co—Co distance is by adopting a displacive modulation described by a linear sawtooth function (Petricek *et al.*, 1990)

$$\mathbf{u} = 2\mathbf{u}_0[(x_4 - x_4^0)/\Delta] \quad \text{for } (x_4^0 - \Delta/2 < x_4^0 < x_4^0 + \Delta/2), \tag{2}$$

where $\mathbf{u}$ is the displacement, $\mathbf{u}_0$ is the maximal displacement and Δ is the definition interval of the sawtooth function.

In Fig. 7 a sawtooth function is plotted in the x_3–x_4 projection, which is important for the description of cobalt along **c**. The function is defined by the centre $x_4{}^0$, by the width Δ and the maximal displacement $\mathbf{u}_0$. For $x_4 = x_4{}^0$, the displacement is 0. With increasing x_4, the displacement increases

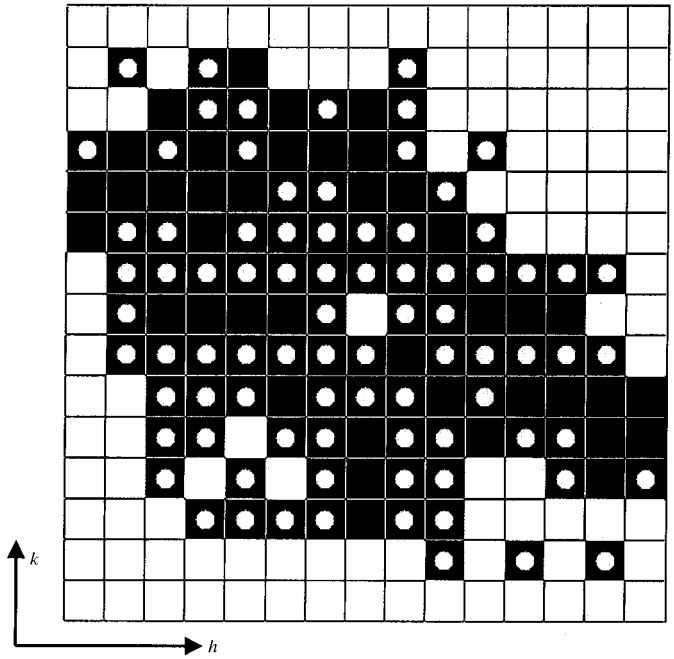

Figure 5
Comparison between X-ray and neutron low-temperature data for the *hk*0 plane. The black squares and white circles indicate measured reflections in the X-ray experiment and in the neutron experiment, respectively.

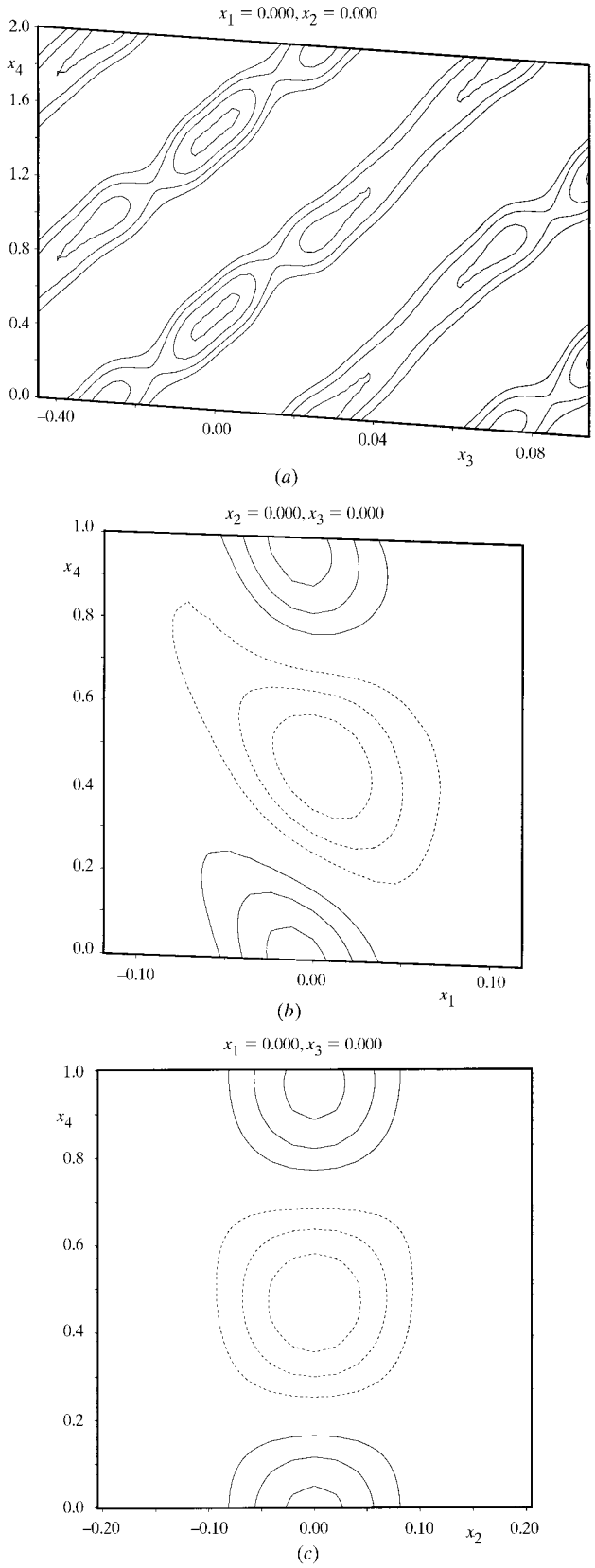

Figure 6
Sections of the four-dimensional Fourier map in the vicinity of Co, indicating the sawtooth type of positional modulation. The contour step is 3 e Å^{-3}, the Fourier coefficient $F_{obs} - F_{calc}$. (*a*) x_3–x_4 section; (*b*) x_1–x_4 section; (*c*) x_2–x_4 section.

linearly until the maximal value $\mathbf{u}_0$. When x_4 reaches point A, the atom disappears and does not exist until point B appears again in the next cell with the opposite maximal displacement $\mathbf{u}_0$.

The sawtooth function describes simultaneously the position and occupation modulation. In real space, the function shown in Fig. 7 generates a row of equally distributed atoms along **c**, which is interrupted by gaps corresponding to locations in superspace where the $\mathbf{R}_3$ section does not intersect the sawtooth function. The row may contain gaps even if case points A and B reach the edges of the elementary cell (*i.e.* $\Delta = 1–2\mathbf{u}_0\mathbf{q}$). The only exception is a sawtooth function with A and B equivalent. This function forming a continuous line in the superspace generates a row of equally distributed atoms in real space without gaps. It is therefore equivalent to a composite model.

3.3. Refinement of modulated structure

3.3.1. Initial sawtooth model solved from X-ray data. In a first step, a positional modulation wave was refined for lanthanum. Owing to the variation of $|\mathbf{q}|$, only the incommensurate approach was used. In the initial refinement, the six twin occupation factors were constrained to the same value of 1/6. Later, the occupation was refined together with the other structural parameters. In the vicinity of cobalt, the difference-Fourier map (Fig. 6) revealed that this atom has a strongly modulated z coordinate, while the x and y modulations are small. The cobalt distribution along a diagonal ridge strongly indicates a composite structure.

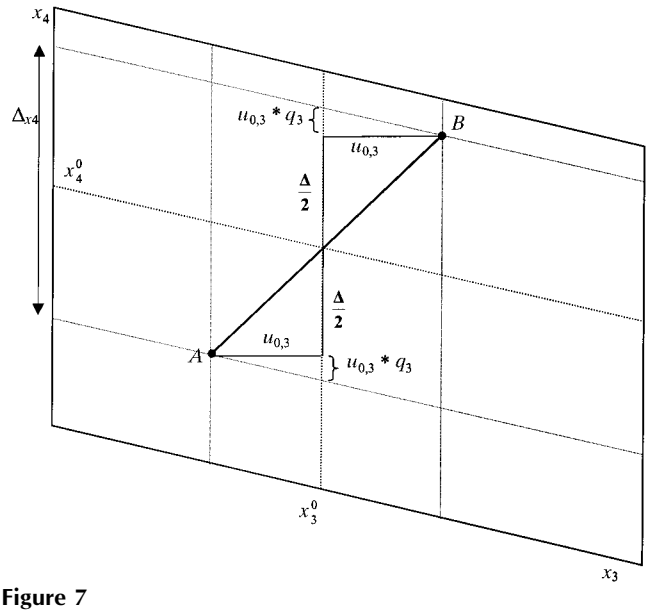

Figure 7
The sawtooth modulation function (abscissa A–B) in the x_4–x_3 projection. Δ, x_4^0 and $u_{0,3}$ define the width of the function, the centre of the function and the maximal displacement from the basic position, respectively. The parameters Δ and $u_{0,x}$ were refined. The centre of the function was located from the Fourier section x_3–x_4 and fixed. The occupation of cobalt is equal to Δ.

Table 4
Final non-weighted R values from the refinement of composite and sawtooth models of La_2Co_{18}.

The symbols LT-S, LT-C, RT-S, RT-C and X are explained at the end of §3.

	All reflections		Main reflections		First-order satellites	
Model	All	Observed	All	Observed	All	Observed
LT-S	0.1493	0.1040	0.0701	0.0667	0.2185	0.1475
LT-C	0.1502	0.1043	0.0768	0.0709	0.2528	0.1707
RT-S	0.1741	0.1198	0.0628	0.0603	0.2811	0.2094
RT-C	0.1750	0.1193	0.0905	0.0687	0.3351	0.2634
X	0.2898	0.2150	0.0817	0.0711	0.4440	0.3545

However, the diffraction pattern did not allow us to draw clear conclusions concerning the composite character of the crystal. The present twinning drastically reduced diffractions from the second Co subsystem for $|l| > 1$ (the second-order satellites were very weak, whereas the third-order ones were not present at all) and therefore only the first layer was clearly detectable (Fig. 11). Moreover, except two sets of main reflections, some pure first-order satellites induced by the modulation of the La atom were present. For these reasons, we focused ourselves initially on the sawtooth model.

The Fourier section shown in Fig. 6 was used to estimate the initial sawtooth parameters. Two sawtooth models were investigated, the first one with cobalt at (0,0,0) and (0,0,$\frac{1}{2}$), and two independent sawtooth functions with the parameters x_4^0 = 0.5, Δ = 0.85; the second one with a single cobalt position at (0,0,$\frac{1}{4}$) and a sawtooth function with the parameters $x_4^0 = 0$, Δ = 0.85. The refinement revealed that the second model with cobalt at (0,0,$\frac{1}{4}$) is more stable than the refinement of the first model. The U^{33} component of the displacement parameter of cobalt dropped to an acceptable value, but the R factor for the first-order satellites was still ∼0.35. Owing to the partial overlapping of the satellites in the X-ray data, the subsequent refinement of the incommensurate structure was performed using the neutron data (see next section) with the well resolved satellites.

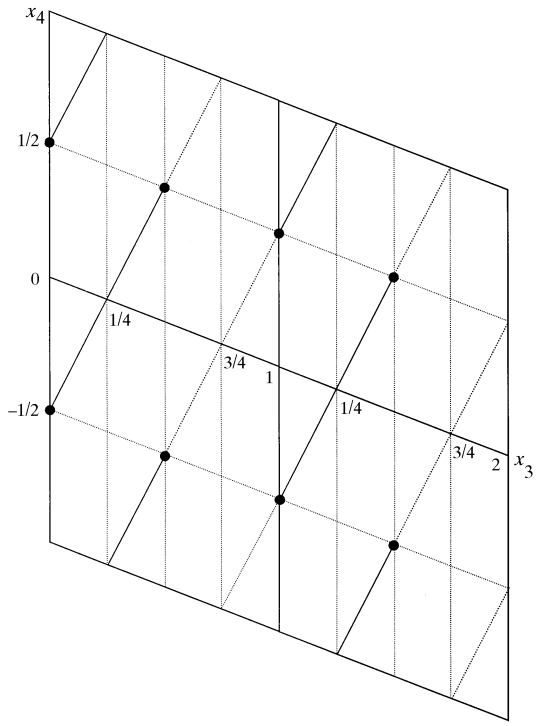

Figure 8
The sawtooth function refined with neutron low-temperature data. The function at (∼0,0,∼$\frac{1}{4}$,0) (solid line) is equivalent with that at (∼0,0,∼$\frac{3}{4}$,0) (dotted line).

3.3.2. The sawtooth model refined with neutron data. The refinement of the low-temperature neutron data, using the structure model resulting from the X-ray refinement, converged to R values 0.104, 0.07 and 0.22 for all observed reflections, main reflections and first-order satellites, respectively (see Table 4 for more details). With an internal R value for the first-order satellites of ∼0.19, this solution reached experimental precision. This model includes one positional modulation wave for lanthanum and a sawtooth function without additional modulation for cobalt. The difference Fourier map still contained puzzling noisy maxima of about 3 e Å^{-3}. Increasing the number of positional and modulation waves did not lead to a significant improvement of the refinement.

The same model applied to the room-temperature neutron data led again to a fit compatible with $R_{\rm int}$ of the first-order satellites (see Tables 2 and 4). The important difference was the shorter definition interval of the sawtooth function. This feature will be discussed in §4.3.

3.3.3. Composite description. The sawtooth function resulting from the refinement with neutron low-temperature data has the width Δ = 0.876 (6) and the maximal displacement $\mathbf{u}_0$ = [0,0,0.251 (1)]. The first component of $\mathbf{u}_0$ was fixed to 0, the second one is 0 from the symmetry. The unrestricted refinement of $\mathbf{u}_0$ converged with $\mathbf{u}_0$ = [0.006 (1), 0, 0.254 (2)] and with R = 0.103 for all observed reflections (*i.e.* lowered by 0.001). With respect to the quality of the data, the restriction of $u_{0,1}$ seems to be a reasonable approximation. Therefore, the sawtooth function can be fully interpreted using the x_4–x_3 section. The refined parameters correspond to a sawtooth function with start- and end-points reaching the edges of the elementary cell. The function (Fig. 8) centred at (∼0,0,∼$\frac{1}{4}$,0), together with the symmetrically equivalent one at (∼0,0,∼$\frac{3}{4}$,0), form a continuous line. This is equivalent to a composite description.

For the composite description, the matrix

$$\mathbf{W} = \begin{pmatrix} 1 & 0 & 0 & 0 \\ 0 & 1 & 0 & 0 \\ 0 & 0 & 2 & -1 \\ 0 & 0 & -1 & 1 \end{pmatrix}$$

was used, defining the relationship of the two subsystems in the reciprocal and direct space as shown in Fig. 12. In reciprocal space, the **c*** axes are not parallel owing to the presence of the wavevector (α, 0, γ). In real space the β angle is different from 90° and the slightly changed **a** axis allow the **c** axes of the first and the second subsystems to coincidence. This arrangement corresponds to the fact that the different

Table 5
Fractional atomic coordinates and equivalent isotropic displacement parameters (Å^2) for La_2Co_{18}.

The symbols LT-S, LT-C, RT-S, RT-C and X are explained at the end of §3.

$$B_{eq} = \Sigma_i \Sigma_j U^{ij} a^i a^j \mathbf{a}_i \mathbf{a}_j$$

Atom	Model	x	y	z	B_{eq}
La	LT-S	0.1684 (1)	0.5	0.2538 (2)	0.0029 (2)
	LT-C	0.1683 (1)	0.5	0.2536 (2)	0.0028 (3)
	RT-S	0.1660 (1)	0.5	0.2479 (3)	0.0158 (4)
	RT-C	0.1679 (1)	0.5	0.2542 (3)	0.0153 (4)
	X	0.1675 (1)	0.5	0.2454 (1)	0.0287 (3)
Co	LT-S	−0.0026 (4)		0.2530 (7)	0.013 (1)
	LT-C			0.5	0.046 (1)
	RT-S	−0.0036 (5)		0.255 (1)	0.033 (2)
	RT-C			0.5	
	X	−0.0107 (1)		0.2478 (3)	0.0101 (4)

Table 6
Anisotropic displacement parameters U^{ij} (Å^2) for La_2Co_{18}.

The symbols LT-S, LT-C, RT-S, RT-C and X are explained at the end of §3. The anisotropic displacement factor exponent takes the form $-2\pi^2 \Sigma_i \Sigma_j U^{ij} a^i a^j h_i h_j$.

Atom	Model	U^{11}	U^{22}	U^{33}	U^{12}	U^{13}	U^{23}
La	LT-S	0.0009 (5)	0.0032 (5)	0.0045 (2)	0	−0.0005 (3)	
	LT-C	0.0008 (5)	0.0032 (5)	0.0044 (2)	0	−0.0004 (3)	0
	RT-S	0.0069 (6)	0.020 (1)	0.0202 (3)	0	−0.0039 (5)	0
	RT-C	0.0069 (5)	0.019 (1)	0.0197 (3)	0	−0.0043 (5)	0
	X	0.0333 (7)	0.0199 (5)	0.0329 (2)	0	−0.0035 (4)	0
Co	LT-S	0.0062 (7)	−0.0017 (6)	0.036 (3)	0	0.0026 (6)	0
	LT-C	0.0072 (7)	−0.0014 (6)	0.041 (2)	0	0.0019 (6)	0
	RT-S	0.0176 (9)	0.0023 (9)	0.078 (5)	0	0.0052 (8)	0
	RT-C	0.0206 (9)	0.0034 (9)	0.113 (3)	0	0.0017 (8)	0
	X	0.0087 (5)	0.0196 (4)	0.002 (1)	0	0.0056 (3)	0

periodicity of cobalt is expected along the **c** axis of the average structure (see Fig. 4). The length of the **c** axis in the second subsystem, 2.38 Å, is close to the minimum allowed Co—Co distance.

In the second subsystem, the cobalt position transformed to $(0,0,\frac{1}{2})$. The symmetry of both subsystems is identical, *i.e.* $C2/m(\alpha 0 \gamma)$. The refinement of the composite model for neutron low-temperature data converged with similar R values (see Table 4) and with parameters similar to the sawtooth model. Here too lanthanum has been refined with one harmonic position modulation wave, whereas cobalt has not been modulated.

The results of the structure refinements are summarized in Tables 1–8. The labels used in the tables characterize the different data sets and models: LT-S (neutron low-temperature, sawtooth); LT-C (neutron low-temperature, composite); RT-S (neutron room-temperature, sawtooth), RT-C (neutron room-temperature, composite) and X (X-ray room-temperature sawtooth).

4. Discussion

4.1. The partial structure of the Co atoms

As previously mentioned in the *Introduction*, the distance between two Co atoms must be larger than one half of the lattice constant c. However, because the x coordinate of cobalt is close to 0 and y is fixed to 0 by symmetry, the distance of two adjacent Co atoms in the basic structure is just $\frac{1}{2}c$. One way for cobalt to achieve a proper distance is by adopting a displacive modulation (described by the sawtooth function) relative to the periodicity of the La atoms along the c axis. In Fig. 9(*a*) the displacements represented by the lines d_1 and d_2 of the cobalt z coordinate from the basic positions $(x,0,z)$ and $(-x,0,-z)$, respectively, are plotted as a function of t. For $t = 0$ the displacement d_1 is positive, while d_2 is negative and its size is equal to d_1. With x close to 0 and z close to 1/4, the approximate Co—Co distance is $\frac{1}{2}c + 2d_1 = 2.36$ Å, which is a plausible distance. Since the two lines d_1 and d_2 are parallel, the distance 2.36 Å is maintained over the entire definition interval of both sawtooth functions.

The Co—Co distance as a function of t is given in Fig. 9(*b*). The abbreviations d_1 and d_2 again differentiate between the (symmetrically dependent) positions $(x,0,z)$ and $(-x,0,-z)$. The two slightly different distances d_1–d_2 arise from the fact that the x and z coordinates in the superspace group $C2/m(\alpha 0 \gamma)$ can vary and are slightly different from 0 and 0.25, respectively. The distance d_1–d_1 occurs when the displacement of d_1 becomes large and positive, and negative values exist for equivalent t coordinates, for instance $t = 0.35$ and $t = 0.65$. The Co—Co distances are always larger than those in the basic structure (dashed lines in the figure).

The best way of modelling the different periodicity of cobalt and lanthanum is the composite description discussed in §3.3.3. Here a plausible Co—Co distance is achieved in the cell of the cobalt subsystem. Provided that the sawtooth model generates rows of cobalt without gaps, the sawtooth and composite descriptions are completely equivalent. The objection against the composite description may be that the higher-order satellites forming the composite periodicity are not observable. This was the main reason why the sawtooth model was first taken into account. However, the composite description is justified by the results obtained for the sawtooth refinement. The reason for the very weak satellites is the presence of the sixfold twinning, leaving the main reflections invariant. The intensity of the main reflections from the six twin domains is cumulated, while each satellite intensity results from a single twin domain.

The refinements in the superspace indicate that the La subsystem is modulated (see Table 7), while the Co subsystem is not. This is a further differentiation of the original model proposed by Schweizer *et al.* (1971). An additional check of the translation properties of the Co subsystem might be offered by the peak topology in the magnetic ordered state. The low-temperature diffraction aspect should be fully described by the Co lattice and the magnetic wavevector (1/3 1/3 0).

Fig. 10 compares the modulated (column Co—S) and basic (Co—B) positions of cobalt in the sawtooth low-temperature model. In this plot, the basic positions described in Fig. 9 as d_1

Table 7
Modulation amplitudes (Å) for La_2Co_{18}.

The symbols LT-S, LT-C, RT-S, RT-C and X are explained at the end of §3. The Fourier series $u_i = \sum_n A_{n,i} \sin(2\pi n \bar{x}_{s4}) + B_{n,i} \cos(2\pi n \bar{x}_{s4})$ represents the modulation function of lanthanum, with $i = 1, 2, 3$ being the three space directions and n the number of modulation waves. The sawtooth function of cobalt is defined in equation (2), and the meaning of the symbols $u_{0,3}$ and Δt is shown in Fig. 7.

Atom	Model	$A_{1,1}$(La) or $u_{0,3}$(Co)	$A_{1,2}$(La) or Δ(Co)	$A_{1,3}$(La)	$B_{1,1}$	$B_{1,2}$	$B_{1,3}$
La	LT-S	−0.0060 (1)		0.0234 (2)	−0.00071 (8)		0.0009 (1)
	LT-C	−0.0060 (1)		0.0234 (2)	−0.00068 (8)		0.0008 (1)
	RT-S	−0.0035 (1)		0.0190(2)	−0.00109 (9)		−0.0007 (2)
	RT-C	−0.0040 (1)		0.0190 (2)	−0.00075 (9)		−0.0001 (2)
	X	0.00053 (6)		0.03040 (9)	0.00141 (8)		−0.0018 (1)
Co	LT-S	0.251 (1)	0.876 (6)	–	–	–	–
	LT-C	–	–	–	–	–	–
	RT-S	0.243 (3)	0.779 (7)	–	–	–	–
	RT-C	–	–	–	–	–	–
	X	0.2673 (5)	0.818 (1)	–	–	–	–

Table 8
Twin fractions (%) refined for La_2Co_{18}.

The symbols LT-S, LT-C, RT-S, RT-C and X are explained at the end of §3.

Model	Domain I	Domain II	Domain III	Domain IV	Domain V	Domain VI
LT-S	19	14	17	14	14	22
LT-C	19	14	17	14	14	22
RT-S	16	16	19	17	15	17
RT-C	16	16	19	17	15	17
X	12	13	23	22	15	15

Table 9
The selected distances (Å) in La_2Co_{18}.

The distances d_{min}, d_{max} and d_{av} were calculated from all 100 equidistant values of t between 0 and 1 where the atom existed. The d_{bas} is the distance in the basic structure, *i.e.* without taking into account the modulation. The symbols LT-S, LT-C, RT-S and RT-C are explained at the end of §3.

Model	Atoms	d_{min}	d_{max}	d_{av}	d_{bas}	$d_{max} - d_{min}$	$d_{av} - d_{basic}$
LT-S	La–Co	2.791	2.966	2.865	2.782 (4)	0.175	0.084
		2.835	3.040	2.916	2.836 (2)	0.205	0.079
	Co–Co	2.359	2.359	2.359	2.111 (5)		0.248
		2.411	2.411	2.411	2.162 (5)		0.249
LT-C	La–Co	2.811	–	–	2.804	–	–
		2.824	–	–	2.825	–	–
	Co–Co	2.378	2.378	2.378	2.378 (0)		
RT-S	La–Co	2.814	2.983	2.876	2.796 (4)	0.170	0.080
		2.830	3.045	2.907	2.834 (2)	0.215	0.074
	Co–Co	2.364	2.364	2.364	2.095 (7)		0.269
		2.452	2.452	2.452	2.180 (7)		0.272
RT-C	La–Co	2.821	–	–	2.811	–	–
		2.825	–	–	2.826	–	–
	Co–Co	2.378	2.378	2.378	2.378 (0)		

and d_2 are indicated by hatched and white circles, respectively. The arrows show the displacement from the basic positions. The basic positions without the corresponding modulated positions are marked as missing. The most important feature is that cobalt exhibits a periodicity along **c**, which is incommensurate with the periodicity of the basic positions. Another interesting feature is the gap between the fifth and sixth basic positions, which is probably an artefact owing to the definition interval of the sawtooth function. This parameter results from a least-squares refinement and is associated with an uncertainty. Close to the 15th basic position, there are two neighbouring white circles. This is an example of a *b*–*b* distance, which is equivalent to the *a*–*a* distances shown in Fig. 9(*b*).

The lanthanum modulation was refined with a single harmonic wave with the largest displacement in the **c** direction. Fig. 10 shows the comparison between the basic (La—B) and modulated (La) positions of lanthanum and its relation to the cobalt displacement. In the average structure (Fig. 3) lanthanum never has the same z coordinate as cobalt. Owing to the different periodicity, cobalt is continuously shifted with respect to lanthanum in the modulated structure and in some cases both atoms have the same z coordinate. Fig. 10 shows that the minimal lanthanum modulation occurs when it is located in the middle of two successive Co atoms and maximal when its z coordinate is close to that of cobalt. The displacements of lanthanum and cobalt have opposite signs so that the Co—La distance is always larger or equal to the distance in the basic structure (see Table 9). The modulation of lanthanum can be considered as a secondary phenomenon arising as a response to the periodicity of cobalt. As expected, the same R values result when a model with opposite signs of the lanthanum modulation parameters and a simultaneous shift by $\frac{1}{2}$ at the centre of the sawtooth function is used (this changes the signs of the cobalt displacement).

The composite model predicts that the magnetic $hk0$ reflections observed at 15 K should be strong, and that the magnetic satellites in the layer $hk2 - q$ should be significant, as their intensities depend only on the Co atoms [for the magnetic reflections $hkl - q$ the following conditions are observed in the hexagonal system: $|h|, |k| = (3n \pm 1)/3$]. In addition, the magnetic satellites in the layers $hk2 + q$, $hk1 - q$ and $hk1 + q$ should be absent if there is no modulation of the Co atomic positions. These predictions are found to be correct (Wilkinson *et al.*, 2000), reinforcing the case for a composite model without Co positional modulation. There is, however, evidence of some very weak magnetic reflections with indices $hk1$ and $hk2$. These are predicted to be systematically absent in the composite model without Co modulation, leaving open the possibility that a very small amplitude of modulation exists. Attempts to fit such a modulation in the refinement of the nuclear structure did not significantly improve the fit, as

the size of the predicted effects almost certainly lies below the level of precision of the observed data.

4.2. Chemical composition

The stoichiometry of the composite model calculated as the ratio of cell volumes of the first and the second subsystem is $La_2Co_{1.80}$. The composition estimated from the sawtooth model refinement (see Δ in Fig. 7 and Table 7) is $La_2Co_{1.752\ (6)}$. This value must be treated with caution. It is associated with the width of the sawtooth function, which is the result of a refinement and is subject to an error. Moreover, this parameter correlates with U^{33} of cobalt and may also be influenced by possible disorder (see §4.3) and by the poor quality of the satellite reflections. On the other hand, the ratio of the cell volumes in the composite is directly derived from the q vector. Provided that the cobalt positions are fully occupied (*i.e.* the rows of cobalt along the c axis do not contain gaps), the stoichiometry $La_2Co_{1.80}$ is the most probable value. It also corresponds to the composition estimated from neutron powder data (Wilkinson *et al.*, 2000).

The discussion about the chemical composition is further complicated by the variation of **q** found for different samples (see §2.4). In the composite model the volume of the second subsystem is 98.3, 96.2 and 94.2 Å^3 for **q** vectors (0.113,0,0.203), (0.08,0,0.165) and (0.06,0,0.134), respectively,

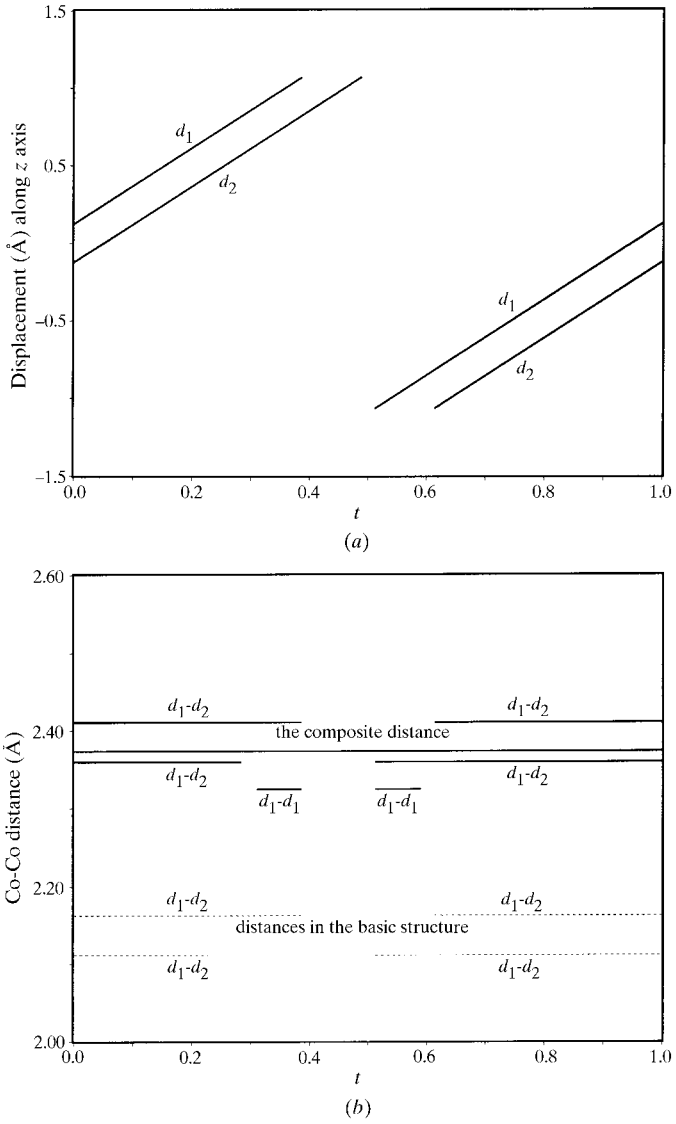

Figure 9
(*a*) The displacement of cobalt along z and (*b*) the Co—Co distance as a function of t. The letters d_1 and d_2 denote the $(x,0,z)$ and $(-x,0,-z)$ positions of cobalt, respectively. The variation of z is expressed as the distance between the basic and modulated coordinate. The dashed line represents the distances in the basic structure.

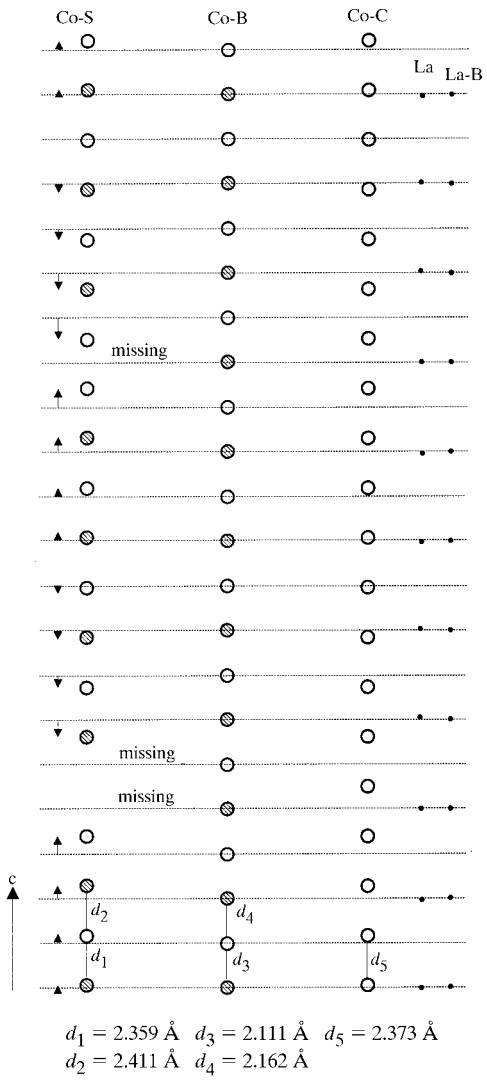

Figure 10
$La_2Co_{1.8}$ modulations in the c direction refined with the neutron low-temperature data. Co—S, Co—B, Co—C, La and La—B represent the columns along the c axis of cobalt in the sawtooth model, cobalt in the basic structure, cobalt in the composite model, lanthanum in the sawtooth model and lanthanum in the basic structure, respectively. The arrows indicate the shifts of cobalt in the sawtooth model with respect to the nearest basic position. The white and hatched circles indicate Co atoms generated from the basic position $(x,0,z)$ and $(-x,0,-z)$, respectively. The horizontal distance of the columns and their order is arbitrary, without connection to the real structure.

expressed in hexagonal coordinates. The corresponding compositions are $La_2Co_{1.80}$, $La_2Co_{1.84}$ and $La_2Co_{1.87}$. We have not systematically tested the **q** vectors so that compositions with less than 1.80 of Co atoms per cell of the first subsystem can also be expected. Therefore, the proper formula is $La_2Co_{1.8\ (1)}$.

4.3. The difference between low- and room-temperature models

The width of the sawtooth function refined with neutron room-temperature data is significantly shorter in comparison to that of the low-temperature data (see Table 7). The resulting composition $La_2Co_{1.56}$ is in variance to that found for the same crystal at low temperature. The refinement of the composite model based on room-temperature data converged to the same ratio R as the sawtooth model (see Table 4), despite the different composition imposed by the composite model description. The high U^{33} displacement parameter (see Table 6) in the composite model indicates a possible disorder of the cobalt subsystem at room temperature. This disorder influences in turn the estimation of the sawtooth width and consequently limits greatly the validity of the predicted composition. The disorder is expected to decrease at low temperature. Indeed, the low-temperature composite model yielded a reasonable parameter U^{33} for cobalt and the predicted composition converges towards the value based on the composite model description. The same anomaly of U^{33}

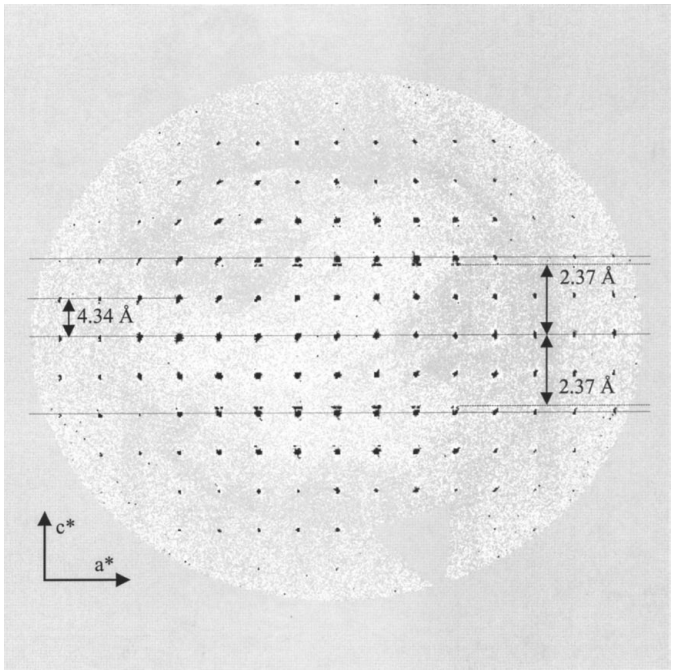

Figure 11
The superposition of the planes (hkl), $k = i - q_x$, i, $i + q_x$, $i = -4$, -3,...,0,...,4, reconstructed from the CCD images with the *KM4CCD* software (Kuma Diffraction, 1999). The distance of the strongest line of the first-order satellites from the origin corresponds to the expected Co—Co distance and indicates that the periodicity of Co atoms along **c*** is different from the periodicity given by the main reflections.

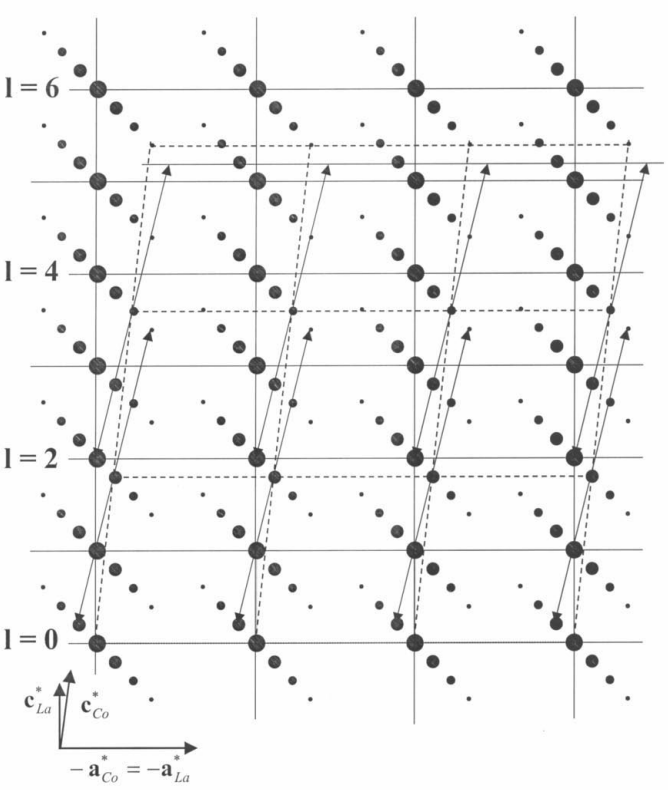

Figure 12
(*a*) The idealized reciprocal space of one twin domain of $La_2Co_{1.8}$, showing the relationship between the elementary cells of two composite subsystems. The full and dotted lines indicate the cell of lanthanum and cobalt, respectively. The arrows show the direction of the **q** vector in the cobalt subsystem. (The **q** vector of the lanthanum cell is not represented, but the following relation holds $\mathbf{q}_{Co} + \mathbf{q}_{La} = \mathbf{c}_{Co}^*$.) The high-order satellites were not observed, but they were included for clarity. For the same reason, the **a*** component was doubled. (*b*) The relationship between elementary cells of the two composite subsystems in direct space. The cell parameters of the first (shaded polygon) and the second (dashed lines) subsystems are $a = 8.4611$, $b = 4.885$, $c = 4.273$ Å, $\beta = 90°$ and $a = 8.478$, $b = 4.885$, $c = 2.378$ Å, $\beta = 86.37°$, respectively.

was also observed for X-ray data collected with a different sample. In both cases, however, we were unable to propose a plausible description of this disorder, which is probably beyond the resolution of our experiment.

4.4. Twin fractions

For all models discussed here the twin fractions have also been refined (see Table 8). The estimated standard deviation of the twin fractions was ~0.2% and their refinement typically decreased R by 0.1 for all observed reflections, 0.05 for main reflections and 0.2 for the first-order satellites. The main reflections are invariant with respect to the twinning operations contrary to the satellites, which are independent in each twin domain. However, the low precision of the satellite intensities makes the twin domain refinement inaccurate. The large difference in the twin fractions for neutron and X-ray data indicates that for X-rays, the results are strongly influenced by absorption effects.

5. Conclusions

The crystal $La_2Co_{1.8\ (1)}$ can be equivalently described by the sawtooth, as well as by the composite model. The composite model is more convenient and simpler for the description of the periodicity of cobalt along the c axis. However, the sawtooth description is justified also, in particular it shows the close relation between the two types of refinements and authorizes the composite model under conditions not ideal for composite refinement. The sawtooth model represents a limiting case at the intersection between the composite and incommensurately modulated models. It should be noted that in these structure refinements, the fit of the first-order satellites is sufficient only for the most pronounced structural features.

The intensities of magnetic reflections observed at 15 K support the composite model, although the existence of a very small modulation of the Co atomic positions cannot be ruled out.

The most probable stoichiometry $La_2Co_{1.80\ (1)}$ is based on the composite model description, taking into account the variation of **q** for different samples. The calculated chemical composition based on the sawtooth model varies largely with the same crystal at different temperatures and consequently cannot be considered as reliable. This is associated with a possible disorder of the Co atoms, which exhibit large correlations of the anisotropic displacement parameters along **c**.

The aim of this work was also to test the usability of neutron data collected with the white-beam Laue technique. The precision of this type of experiment is comparable with other data collection techniques used for diffraction experiments. However, special attention has to be paid to the incompleteness of the Laue data. This can be overcome by performing a restricted waveband (quasi-Laue) experiment (Wilkinson *et al.*, 2000) or by measuring low-order data in a monochromatic (very narrow waveband) experiment. In the present work we overcame this problem by using the X-ray data in order to find the initial structural model, which was further refined with more precise neutron data.

We gratefully acknowledge the Swiss National Science Foundation (grants 20-46666.96 and 20-56870.99) for supporting this project. The Grant Agency of the Academy of Sciences of the Czech Republic (grant A1010901) and the Grant Agency of the Czech Republic (grant 202/00/0645) is also gratefully acknowledged. We thank Dr Mathias Meyer for assistance with the X-ray experiments.

References

Ballou, R., Gignoux, D., Lemaire, R., Mendia-Monterroso, R. & Schweizer, J. (1986*a*). *J. Magn. Magn. Mater.* pp. 54–57.
Ballou, R., Gignoux, D., Lemaire, R., Mendia-Monterroso, R. & Schweizer, J. (1986*b*). *J. Magn. Magn. Mater.* pp. 499–500.
Ballou, R., Gignoux, D., Lemaire, R. & Schweizer, J.(1987). *Acta Phys. Pol. A*, **72**, 25–28.
Cipriani, F., Castagna, J.-C., Wilkinson, C., Oleinek, P. & Lehmann, M. S. (1996). *J. Neutron Res.* **4**, 79–85.
Kuma Diffraction (1999). *KM4CCD System Software*, Version 1.162. Kuma Diffraction Instruments and Université de Lausanne, Switzerland.
Nam, D. N. H., Tung, L. D., Nordblad, P., Thuy, N. P. & Phuc, N. X. (1998*a*). *J. Magn. Magn. Mater.* pp. 177–181.
Nam, D. N. H., Tung, L. D., Nordblad, P., Thuy, N. P. & Phuc, N. X. (1998*b*). *J. Magn. Magn. Mater.* pp. 1135–1136.
Petricek, V. & Dusek, M. (1998). *JANA*98. Institute of Physics, Praha, Czech Republic.
Petricek, V., Gao, Y., Lee, P. & Coppens, P. (1990). *Phys. Rev. B*, **42**, 387–392.
Schweizer, J., Strnat, K. A. & Tsui, J. (1971). 9th Rare Earth Research Conference, Blacksburg, Virginia, USA.
Stoe & Cie (1996). *X-Shape*, Version 1.01. Stoe and Cie, Darmstadt, Germany.
Weisgerber, S. & Helliwell, J. R. (1993). *J. Chem. Soc. Faraday Trans.* **89**, 2667–2775.
Wilkinson, C., Schobinger-Papamantellos, P., Myles, D., Tung, L. D. & Buschow, K. H. J. (2000). *J. Magn. Magn. Mater.* **217**, 55–64.